CONFORMAL MAPS FOR THE DISCRETIZATION OF ANALOG FILTERS NEAR THE NYQUIST LIMIT

Champ C. Darabundit and Jonathan S. Abel

Center for Computer Research in Music and Acoustics
Stanford University
Stanford, CA
champ@ccrma.stanford.edu | abel@ccrma.stanford.edu

ABSTRACT

We propose a new analog filter discretization method that is useful for discretizing systems with features near or above the Nyquist limit. A conformal mapping approach is taken, and we introduce the peaking conformal map and shelving conformal map. The proposed method provides a close match to the original analog frequency response below half the sampling rate and is parameterizable, order preserving, and agnostic to the original filter's order or type. The proposed method should have applications to discretizing filters that have time-varying parameters or need to be implemented across many different sampling rates.

1. INTRODUCTION

Accurate analog filter discretization is a common concern when digital filters are derived from prototype filters or when modeling analog audio effects [1–5]. Once the characteristics of an analog system are known, a method for discretization which maps the Laplace transform s-Plane onto the Z-transform z-Plane is often used to derive a representation of the analog system in the digital domain [6, 7].

The bilinear transform is a popular discretization method, which maps the highest and lowest continuous frequencies to the highest and lowest discrete frequencies exactly once. As there is a direct one-to-one mapping from the s-Plane to the z-Plane, the bilinear transform avoids aliasing and preserves order and stability in the discretized system [6]. However, a byproduct of mapping infinite continuous frequencies to a finite range of digital frequencies is frequency warping. This distorts the original response and is particularly severe near the half the sampling rate: the Nyquist limit. A technique known as "prewarping" allows for some correction of the effects of frequency warping by directly mapping one continuous frequency to one discrete frequency, but it will not completely correct for frequency warping near the Nyquist limit [8].

A standard approach when discretizing analog filters with features near or above the Nyquist limit is to oversample and perform the processing at a higher sampling rate before downsampling back to the original sampling rate [9]. This approach can be disadvantageous as it requires more cycles and special care taken to avoid aliasing. Another option is to use optimization methods, such as least squares [10–12] or warped filter design methods [13], to derive a digital response which closely matches the desired analog response below the Nyquist limit. These approaches, though optimal, are not ideal in cases where there are time-varying filter parameters, as they are computationally intensive and require offline processing to compute interpolatable coefficient tables. A separate approach is to reconstruct the desired continuous-time signal using Shannon's interpolation theorem, but this technique suffers from poor resolution near the Nyquist limit [14]. Another set of methods aims to modify the original prototype filter design to account for frequency warping such that, when discretized, the resulting response more closely matches the desired prototype response. These approaches either attempt to adjust the quality factor (Q) of the prototype filter [15–17] or match the asymptotic high frequency gain to the prototype Nyquist limit gain [18, 19]. These methods, however, are limited to specific filter designs and require some knowledge of the original prototype filter's construction.

In this paper, we propose a new method for discretizing known analog systems through the use of conformal mapping. Conformal maps are complex functions which map a simply connected domain onto another simply connected domain [20] and have a wide range of applications in audio signal processing. The bilinear transform, which maps the complex s-domain to the complex z-domain, is a conformal map in the family of Möbius transformations [20, 21]. Conformal maps are utilized in the field of warped filter design [22, 23] and other discretization methods, such as the bark scale bilinear transform [8]. Conformal maps are sometimes referred to as spectral transforms and are used to design lowpass, highpass, bandpass, and bandstop filters from prototype lowpass filters [24,25]. We will highlight a use for conformal maps as spectral transforms outside of these specific cases and derive peaking and shelving conformal maps. These new conformal maps will allow us to discretize analog systems with behavior near the Nyquist limit, and a matrix representation of said conformal maps will aid us in applying and inverting them.

The paper is structured as follows. Section 2 will review the definition of the bilinear transform and the work done by [18], Section 3 will explore conformal maps and their matrix representation, Section 4 will derive the peaking and shelving filter conformal map. In Section 5, the approach to using said conformal maps for discretization will be demonstrated and compared to existing methods, and Section 6 will conclude.

2. REVIEW OF DISCRETIZATION

2.1. The bilinear transformation

The bilinear transformation can be viewed as a substitution from the continuous-time s-Plane to the discrete-time z-Plane where the

forward and inverse transformation are defined as [6]:

$$s = c\frac{1-z^{-1}}{1+z^{-1}} \qquad z^{-1} = \frac{1+s/c}{1-s/c} \tag{1}$$

where c is the bilinear constant, which is normally

$$c = \frac{2}{T} \tag{2}$$

and $T = 1/f_s$ and f_s is our sampling rate. If a perfect mapping from a singular analog frequency Ω to a digital frequency ΩT is desired, then c is modified to

$$c = \frac{\Omega}{\tan(\Omega T/2)} \tag{3}$$

2.2. Review of prior work

In [18], Orfanidis compensates for the effects of frequency warping in the bilinear transform by adjusting the prototype filter such that the asymptotic high frequency gain matches the gain at the Nyquist limit. This is done because the bilinear transform maps the gain at infinite frequency to the gain at the highest digital frequency, the Nyquist limit. A similar approach can also be found in [19].

We will utilize the same shorthand as Orfanidis to distinguish continuous-time frequencies in Hertz and rad/seconds, and discrete-time frequencies in rads/sample. Say, for our sampling rate f_s in Hz, we express the equivalent frequencies in rad/s and rads/samples by copying the subscript.

$$\Omega_s = 2\pi f_s, \quad \omega_s = \frac{2\pi f_s}{f_s} = 2\pi \tag{4}$$

The analog prototype in [18] has the parameters $\{f_c, \Delta f, G_0, G_C, G_B\}$ which correspond to the boost/cut peak frequency, the bandwidth of the peak, the gain at dc, the gain at f_c, and the bandwidth gain. The corresponding transfer function is:

$$H(s) = \frac{G_0 s^2 + Bs + G_0\Omega_0^2}{s^2 + As + \Omega_0^2} \tag{5}$$

where

$$A = \sqrt{\frac{G_B^2 - G_0^2}{G_C^2 - G_B^2}}\Delta\Omega, \quad B = G_C A \tag{6}$$

Orfanidis then modifies the transfer function to

$$H'(s) = \frac{G_1 s^2 + Bs + G_0 W^2}{s^2 + As + W^2} \tag{7}$$

H' is now dependant on the parameter G_1, the magnitude of (5) at the Nyquist limit, and W, which is a parameter related to, but not equal to Ω_0. W can be found by solving the following set of equations

$$\frac{d}{d\Omega}|H'(\Omega_c)|^2 = 0, \; |H'(\Omega_c)|^2 = G_C^2, \; |H'(\Omega_{1,2})|^2 = G_B^2 \tag{8}$$

The first equation enforces the requirement that the boost/cut peak is located at Ω_c, the second equation requires the magnitude at Ω_c is still G_C, and at the analog bandedges $\Omega_{1,2}$ ($\Delta\Omega = \Omega_2 - \Omega_1$) the gain is still G_B. The bilinear transform is applied to the transfer function in (7) and Orfanidis prewarps the bilinear transform based on the bandwidth. The result of these corrections is shown

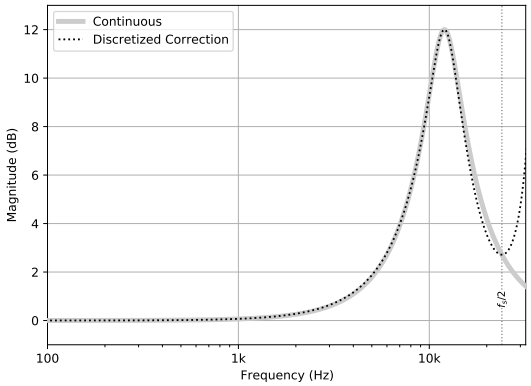

Figure 1: *Correction of peaking equalizer as done in [18]. f_s = 48 kHz*

in Figure 1 where we have $G_0 = 0$ dB, $G_C = 12$ dB, $\omega_c = 0.5\pi$, $\Delta\omega = 0.2\pi$, and $G_B = 9$ dB. What is critical in approaches like Orfanidis', where a prototype filter is modified in anticipation of discretization, is that the discretized response matches the analog response below the Nyquist limit and that it is formed by designing a modified analog prototype.

3. CONFORMAL MAPPING

Conformal maps are complex functions which map a simply connected domain onto another simply connected domain by composing the conformal mapping function with an analytical function. In the case of a discrete transfer function H and conformal mapping function g, a mapped transfer function H' is derived by

$$H'(z^{-1}) = (H \circ g)(z^{-1}) = H(g(z^{-1})) \tag{9}$$

where $\circ$ defines function composition. In this paper, we will notate the application of a conformal map as a substitution, like so

$$z^{-1} \leftarrow g(z^{-1}) \tag{10}$$

A class of conformal maps in the digital domain, which are particularly useful to us, is the allpass transformation.

$$g(z^{-1}) = e^{j\theta}\prod_{i=1}^{n}\frac{p_i - z^{-1}}{1 - p_i z^{-1}} \tag{11}$$

p_i is the pole location of each 1st-order section, and n is the order of the conformal map. The allpass transformation is in fact a digital allpass filter. When used as a conformal map, the allpass filter's unity gain results in points on the unit circle being mapped to other points on the unit circle through warping only their angle.

The order of a conformal map determines the resulting order of the transformed system. First order conformal maps have the property of being order preserving, while higher order mappings will increase the order by a factor of the conformal map's order [8, 26].

As an example, we will apply what [26] refers to as the "littlest conformal map"

$$z^{-1} \leftarrow g(z^{-1}) = \frac{a + z^{-1}}{1 + az^{-1}} \tag{12}$$

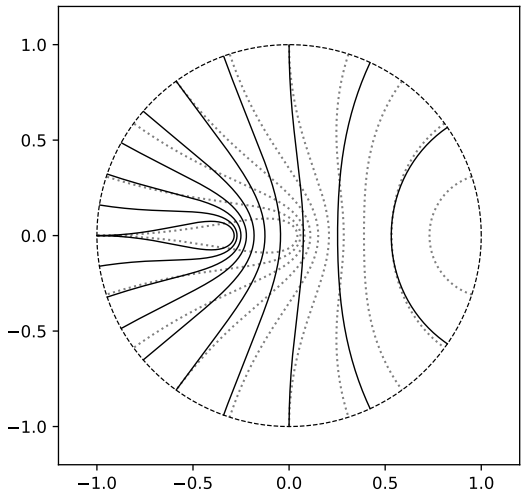

Figure 2: *First order allpass conformal mapping, the dotted lines are constant radius semicircles in the left half of the s-Plane mapped to the z-1-plane by the equivalence* $z = e^{-sT}$. *The solid lines represent the first order mapping in (12) where* 0.3π *is warped to* 0.5π.

$$a = \tan\left(\frac{1}{2}\left(\beta T - \frac{\pi}{2}\right)\right) \tag{13}$$

which is a 1st-order allpass transformation where the coefficient a maps the frequency at $\frac{\pi}{2}$ radians to the frequency at βT radians and β is the continuous-time angular frequency we are mapping to.

We illustrate this transformation in Figure 2, by applying our "littlest" mapping to constant radius semicircles in the left half of the s-Plane that have been transformed to the z-1-Plane by the equivalence $z = e^{-sT}$. We have chosen radii equivalent to $\frac{n}{10}\frac{\omega_s}{2}$ where $n = 1, 2, \ldots 10$, and for our transform we chose $\beta T = 0.3\pi$. Our plot can be read by looking at the increasing radial lines from right to left and noticing that the 3rd solid line — representing our mapping — now intersects with the unmapped 5th dotted line on the unit circle. When applied, the conformal map causes response at 0.3π to be "substituted" by the response at 0.5π.

It is possible to derive a continuous-time equivalent of any discrete-time conformal map by composing our discrete-time conformal map with the bilinear transform and its inverse, and using the frequency warping property of the bilinear transform where $\Omega/c = \tan\left(\frac{\omega}{2}\right)$.

$$c\frac{1 - z^{-1}}{1 + z^{-1}} \leftarrow g(z^{-1}) \leftarrow \frac{1 + s/c}{1 - s/c} \tag{14}$$

The equivalent continuous-time conformal map of the "littlest" mapping is then

$$s \leftarrow g(s) = \frac{\Omega_s}{4\beta}s \tag{15}$$

which intuitively demonstrates when $s = j\beta$, we have $g(s) = j\Omega_s/4$.

By applying this method, we can derive continuous-time equivalents, shown in Table 1, of the generalized discrete-time allpass transformations in [24], unifying them with the continuous-time transforms in [25]. These transforms are well known and are denominated by the effect each mapping has on a lowpass filter [4,24, 25]. Where the shorthands $LP \rightarrow LP$, $LP \rightarrow HP$, $LP \rightarrow BP$, and $LP \rightarrow BS$, refer to the lowpass to lowpass, highpass, bandpass, and bandstop transformations respectively.

Table 1: *General allpass transforms in the s-Plane*

Order	Transform	Analogy	$g(s)$
1	$LP \rightarrow LP$	Shift	$s \leftarrow \frac{\beta}{\Omega_c}s$
1	$LP \rightarrow HP$	Flip	$s \leftarrow -\beta\Omega_c\frac{1}{s}$
2	$LP \rightarrow BP$	Mirror about dc and shift	$s \leftarrow \frac{\beta}{\Omega_2 - \Omega_1}\frac{s^2 + \Omega_o^2}{s}$
2	$LP \rightarrow BS$	Mirror about ∞ and shift	$s \leftarrow \beta(\Omega_2 - \Omega_1)\frac{s}{s^2 + \Omega_o^2}$

For all our transforms, β is the frequency we are mapping from, and, in our 1st-order transforms, Ω_c is the frequency we are mapping to. In our second order transforms, we map β to Ω_1 and Ω_2. And, we have $\Omega_o = \Omega_1\Omega_2$. The advantage of performing these transforms in the s-Plane is that our mappings are no longer bandlimited and we avoid any additional warping that may occur in the z-Plane.

While these transformation are characterized by the effect each mapping has on a lowpass filter, it is worth acknowledging that these transforms can be applied to any type of filter. As such, we provide analogies that reflect the behavior of each conformal map on the frequency axis rather than just how each mapping affects a lowpass filter. Nevertheless, we will continue to refer to these transformation by how they affect a lowpass filter.

3.1. Predicting the bilinear transform

The continuous-time bandstop transform maps frequencies from dc to $+\infty$ to the frequency range from dc to Ω_o such that β is mapped to Ω_1. The response is then geometrically mirrored about Ω_o such that β is also mapped to Ω_2. The compression of an infinite frequency range to a finite one draws similarity to how the bilinear transform maps the s-Plane to the z-Plane. The bilinear transform also has mirrored responses above Nyquist limit as we traverse the lower half of the unit circle in the z-Plane. The difference between these two transforms is that the warping in the bilinear transform is fixed and the mirroring is periodic, occurring at $n\frac{f_s}{2}, n = 1, 2, 3....$

Due to the similarities between these two conformal maps, we can replicate the frequency warping in the first "mirroring" of the bilinear transform using the bandstop conformal map. To do this, we take $\Omega_o = \Omega_s/2$ and then map β to the frequency it would be warped to by the bilinear transform.

$$\Omega_1 = c \cdot \arctan\left(\frac{\beta}{c}\right) \tag{16}$$

where c is the normal definition of the bilinear constant in (2). We then find Ω_2 by geometrically mirroring Ω_1 about Ω_o.

$$\Omega_2 = \frac{\Omega_o^2}{\Omega_1} \tag{17}$$

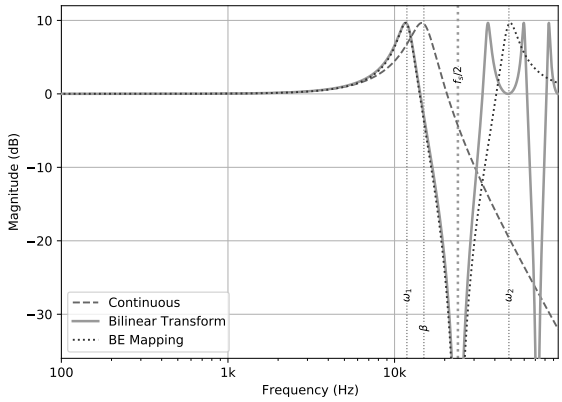

Figure 3: *Bilinear transform and bandstop mapping applied to a resonant lowpass filter. Frequencies above $f_s/2$ demonstrate periodic behavior of the bilinear transform. Frequencies below the $f_s/2$ show the bandstop mapping replicating the behavior of the bilinear transform*

In Figure 3, we use the above parameters and apply a bandstop mapping on a resonant lowpass filter having the transfer function in (18), $f_c = 15$ kHz, and $Q = 3$ to replicate the warping in the bilinear transform below $f_s/2$.

$$H(s) = \frac{1}{\frac{1}{\Omega_c^2}s^2 + \frac{1}{Q\Omega_c}s + 1} \tag{18}$$

As we can replicate the bilinear transform's frequency warping using the bandstop mapping, we can also use the bandstop mapping to better predict frequency warping. Viewed another way: if we can design a filter that closely matches our desired analog response below $f_s/2$ that is geometrically mirrored about our Nyquist limit, and if we can invert said filter with an inverse bandstop mapping, we will derive a filter — upon discretization — that will be a close match to our desired response.

3.2. Matrix representation of conformal maps and their inversion

By necessity, the inverse of a higher order conformal map is a fractional order conformal map. We wish to avoid fractional order filters so we instead rely on a pseudo-inverse derived by representing a conformal map as a transformation matrix.

It was demonstrated in [27], that it is possible to represent a conformal map as a matrix operation on filter coefficients. First, we define a general IIR transfer function in the s-Plane.

$$H(s) = \frac{(0)s^M + (0)s^{M-1} \cdots + b_N s^N + \cdots + b_0}{a_M s^M + a_{M-1}s^{M-1} \cdots + a_0} \tag{19}$$

Where M and N are the order of our denominator and numerator polynomials, and $M \geq N$. We have zero padded our numerator coefficients so, representationally, the numerator and denominator are polynomials of the same order M. We then have two ordered (M+1) x 1 coefficient vectors $\boldsymbol{a} = \begin{bmatrix} a_M & a_{M-1} & \cdots & a_0 \end{bmatrix}^T$ and $\boldsymbol{b} = \begin{bmatrix} b_M & b_{M-1} & \cdots & b_0 \end{bmatrix}^T$. Then, substituting in a general bandstop mapping,

$$g(s) = \frac{gs}{s^2 + d} \tag{20}$$

for s in our general transfer function and multiplying our numerator and denominator by $(s^2 + d)^M$, we have the bandstop mapped response:

$$H(s) = \frac{b_M g^M s^M + b_{M-1} g^{M-1} s^{M-1} (s^2+d)^1 \cdots + b_0 (s^2+d)^M}{a_M g^M s^M + a_{M-1} g^{M-1} s^{M-1} (s^2+d)^1 \cdots + a_0 (s^2+d)^M} \tag{21}$$

The coefficient map can be found by computing the powers of $(s^2 + d)^m$ using the binomial theorem

$$(s^2 + d)^m = \sum_{k=0}^{m} \binom{m}{k} s^{2k} d^{m-k} \tag{22}$$

and representing each additional multiplication s^{2k} as a skip up two rows in a coefficient transformation matrix. We then have a (2M+1) x (M+1) rectangular matrix which maps an (M+1) x 1 vector of general coefficients $\boldsymbol{c}$ to (2M+1) x 1 conformally mapped bandstop filter coefficients $\boldsymbol{c'}$

$$\begin{bmatrix} 0 & \cdots & 0 & 0 & g^0\binom{M-0}{M}d^0 \\ \vdots & & \vdots & \vdots & \vdots \\ g^M\binom{0}{0}d^0 & \ddots & \vdots & \vdots & \vdots \\ \vdots & & g^2\binom{M-2}{0}d^{M-2} & 0 & g^0\binom{M-0}{1}d^{M-1} \\ & & 0 & g^1\binom{M-1}{0}d^{M-1} & 0 \\ 0 & \cdots & 0 & 0 & g^0\binom{M-0}{0}d^M \end{bmatrix} \begin{bmatrix} c_M \\ c_{M-1} \\ c_{M-2} \\ \vdots \\ c_0 \end{bmatrix} = \begin{bmatrix} c'_{2M} \\ c'_{2M-1} \\ c'_{2M-2} \\ \vdots \\ c'_0 \end{bmatrix} \tag{23}$$

To invert our mapping we utilize a pseudo-inverse matrix. From the formulation of our coefficient transformation matrix we know the columns are linearly independent and the pseudo-inverse will be a left inverse. For the original transformation matrix $\boldsymbol{A}$, we have the pseudo-inverse matrix $\boldsymbol{A}^+$ where

$$\boldsymbol{A}^+ \begin{bmatrix} c'_0 \\ c'_1 \\ c'_2 \\ \vdots \\ c'_{2N} \end{bmatrix} = \begin{bmatrix} c_0 \\ c_1 \\ c_2 \\ \vdots \\ c_N \end{bmatrix} \tag{24}$$

returns our original filter coefficients. We compute $\boldsymbol{A}^+$ using existing methods, such a `pinv` in Matlab or Python. Intuitively, representing a conformal map as a matrix operation on the coefficients applies the equivalent conformal map in the filter coefficient space. The pseudo-inverse approximates the inverse conformal map in the same coefficient space, provided that we parameterize our original transform $\boldsymbol{A}$ correctly.

The pseudo-inverse can only be usefully applied to filters that have been previously mapped by a general bandstop transform as in (20), meaning it must have the mirroring properties defined in (17). Additionally, the mirroring frequency Ω_o must be the same in our forward and pseudo-inverse mappings to ensure that symmetry in the transformation is preserved.

4. PEAKING AND SHELVING ALLPASS TRANSFORMS

As our goal is to match our continuous-time response below the Nyquist limit, we propose a 2nd-order conformal map with real coefficients which generates a peaking — specifically a cut filter — from a lowpass filter. We will design our transformation in the digital domain using the allpass transformation. Designing in the

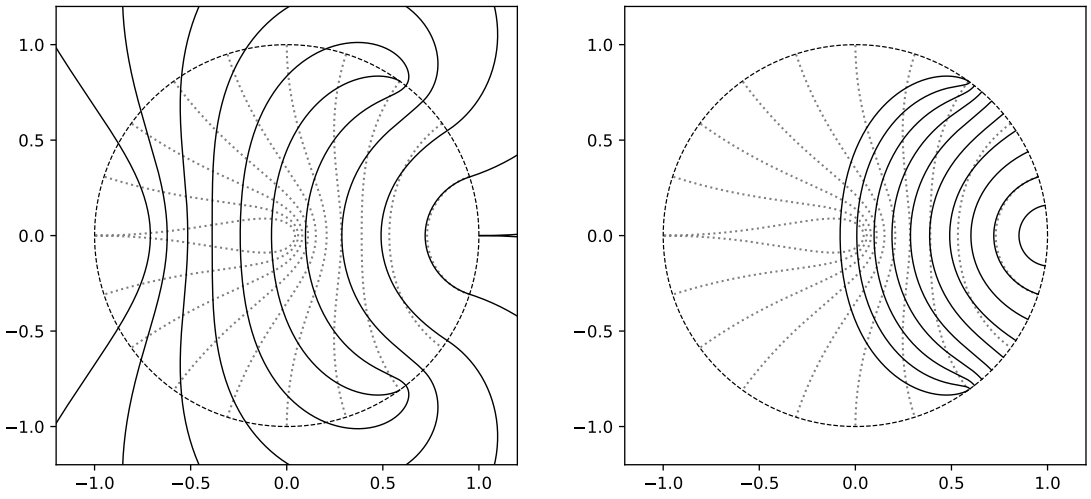

Figure 4: *Left: Peaking conformal map in the z-Plane. The solid lines represent the mapping in (33) where* $\omega_c = 0.3\pi$ *and* $\hat{\omega_o} = \frac{\pi}{2}$*. On the unit circle* 0.3π *is evaluated only once at the 5th constant radial line, signifying the mapping of* 0.3π *to* 0.5π *and zero group delay at that point. The other mapped constant radius lines are evaluated twice on the unit circle around the 5th line.*
Right: Stabilized shelving conformal map in the z-Plane. The inverse mapping of $z^{-1} \leftarrow z^{-2}$ *has been applied to the peaking transformation shown on the left. The constant radial lines are compressed and are only mapped between dc and* 0.3π*, as the frequency response is now truncated to* 0.3π

z-Plane provides an avenue to directly evaluate mappings to infinite frequency in the s-Plane. Additionally, the design of allpass filters is a well explored topic [28] and the form of the allpass filter provides adequate constraint to derive an analytical mapping.

Our desired conformal map will proceed along the unit circle to an angle ω_o and then, effectively, reverse direction to mirror our response. We will demonstrate that a shelving conformal map can be found by applying an inverse bandstop mapping to our peaking conformal map. As with the commonly defined spectral transformations, we designate these conformal maps by their respective effects on a lowpass filter.

4.1. Peaking Allpass Transform

We start with a cascade of two 1st-order allpass sections with possibly complex poles p_1 and p_2

$$g(z^{-1}) = \frac{p_1 - z^{-1}}{1 - p_1 z^{-1}} \frac{p_2 - z^{-1}}{1 - p_2 z^{-1}} \tag{25}$$

Similar to [18], we deduce that for our mapping to peak at ω_o we must have group delay $G(\omega) = -\frac{d}{d\omega}\Theta(\omega_o) = 0$, where $\Theta(\omega)$ is the phase response of our transform. The group delay for a single allpass section is

$$G_1(\omega) = -T \frac{p_1^2 - 1}{p_1^2 - 2p_1 \cos(\omega) + 1} \tag{26}$$

And for our cascaded transformation, our group delay is

$$G(\omega) = -T \left[\frac{p_1^2 - 1}{p_1^2 - 2p_1 \cos(\omega) + 1} + \frac{p_2^2 - 1}{p_2^2 - 2p_2 \cos(\omega) + 1} \right] \tag{27}$$

Setting $G(\omega_o) = 0$, and solving for p_1 in terms of p_2 we have

$$p_1 = \frac{p_2 \cos(\omega_o) - 1}{p_2 - \cos(\omega_o)} \quad \text{or} \quad \frac{1}{p_2} \tag{28}$$

The latter solution represents the case where our transformation is unity and our group delay everywhere is zero. Thus, we choose the former solution for p_1. From the bounds of cos, our solution (28) results in one of our poles appearing outside the unit circle, meaning our mapping is inherently unstable. We will, however, ignore the issue of stability for now.

If one pole exists outside the unit circle, to have real valued coefficients, p_1 and p_2 cannot be complex conjugates and must be real. To simplify our derivation, we request that our peaking frequency $\omega_o = \frac{\pi}{2}$. [26] has pointed the "magic" of $\frac{\pi}{2}$ as it will create a symmetric frequency response, but for our purposes it is also easier to evaluate. We now have

$$p_1 = -\frac{1}{p_2} \tag{29}$$

Substituting in p_1 into (25), and with no loss of generality dropping the subscript in p_2, our 2nd-order mapping is

$$g(z^{-1}) = \frac{-pz^{-2} + (p^2 - 1)z^{-1} + p}{pz^{-2} + (p^2 - 1)z^{-1} - p} \tag{30}$$

We now solve for p by mapping some frequency ω_c to $\frac{\pi}{2}$

$$e^{-j\omega_c} = g(e^{-j\pi/2}) = \frac{p - j(p^2 - 1) + p}{-p - j(p^2 - 1) - p} \tag{31}$$

Solving this equation for p, we find

$$p = \tan\left(\frac{\omega_c}{4}\right) \quad \text{or} \quad -\frac{1}{\tan\left(\frac{\omega_c}{4}\right)} \tag{32}$$

We take the first solution to be our solution for p, as the other solution expresses the relationship between p_1 and p_2 from (29) due to our choice of ω_o. The effect of this mapping is shown in Figure 4. As expected, because our conformal map is unstable, the

mapping causes our previously stable constant radial lines to now also appear outside the unit circle.

By composing the peaking conformal map with the "littlest" conformal map from Sec. 3, we can generalize our peaking transformation further by shifting our peaking frequency $\omega_o = \frac{\pi}{2}$ to some frequency $\hat{\omega}_o$ on the unit circle. Our general peaking filter mapping is

$$g(z^{-1}) = \frac{z^{-2} + \gamma_1 z^{-1} + \gamma_0}{\gamma_0 z^{-1} + \gamma_1 z^{-1} + 1} \tag{33}$$

where

$$\gamma_1 = -\frac{2\cos\left(\frac{\omega_c}{2}\right)}{\cos\left(\frac{2\hat{\omega}_o + \omega_c}{2}\right)} \tag{34}$$

$$\gamma_0 = \frac{\cos\left(\frac{2\hat{\omega}_o - \omega_c}{2}\right)}{\cos\left(\frac{2\hat{\omega}_o + \omega_c}{2}\right)} \tag{35}$$

And, our continuous-time equivalent conformal map is

$$g(s) = -\frac{2\Omega_o \Omega_c s}{s^2 - \Omega_o^2} \tag{36}$$

where Ω_o corresponds to $\hat{\omega}_o$.

Notice that the continuous-time peaking conformal map has the same form as the general bandstop conformal map. As previously mentioned, our peaking conformal map is unstable and any filter produced as a result of this mapping will also be unstable. We can stabilize our system by assuming minimum phase and reflecting any unstable poles and zeros inside the unit circle, in the discrete-time case, or to the left half plane in the continuous-time case.

4.2. Shelving Allpass Transformation

We derive the shelving transform from the peaking transform in both the discrete and continuous domains once the transformed filter has been stabilized. To create a shelving allpass transformation in the z-Plane we make use of the property that any second order allpass transformation is a composition of a shift transformation, a squaring transformation, and another shift transformation [20, 26].

$$g(z^{-1}) = \frac{a + z^{-1}}{1 + az^{-1}} \leftarrow z^{-2} \leftarrow \frac{b + z^{-1}}{1 + bz^{-1}} \tag{37}$$

In the digital domain, we need only apply an inverse squaring mapping to our peaking conformal map in (30) to derive the our shelving filter. To do this we utilize the matrix representation of a conformal map, and notice that the $z^{-1} \leftarrow z^{-2}$ mapping is a (2M+1) x (M+1) rectangular permutation matrix formed from an identity matrix interleaved with rows of zeros, where M is the order of our shelving filter.

$$\boldsymbol{A}_{\boldsymbol{z^{-2}}} = \begin{bmatrix} 1 & 0 & \dots & 0 & 0 \\ 0 & 0 & \dots & 0 & 0 \\ 0 & 1 & \dots & 0 & 0 \\ & & \ddots & & \\ 0 & 0 & \dots & 1 & 0 \\ 0 & 0 & \dots & 0 & 0 \\ 0 & 0 & \dots & 0 & 1 \end{bmatrix} \tag{38}$$

The inverse of a permutation matrix is its transpose. We can derive our digital shelving filter response by applying $\boldsymbol{A}^T_{\boldsymbol{z^{-2}}}$ to our coefficients following a stabilized peaking transform.

In the analog domain, we must compute a pseudo-inverse matrix to invert our peaking transformed filter. We start with the general bandstop transform (20) to compute our forward transform. As required, we set $d = \Omega_o^2$ to match our peaking transformation.

$$g(s) = \frac{gs}{s^2 + \Omega_o^2} \tag{39}$$

We then solve for g such that when $s = j\hat{\Omega}$ we instead map to $s = j\hat{\beta}$.

$$g = \frac{\hat{\beta}}{\hat{\Omega}}(\Omega_o^2 - \hat{\Omega}^2) \tag{40}$$

$\hat{\Omega}$ is the frequency that our original β is mapped to. We find $\hat{\Omega}$ by substituting in β to (36) and choosing the lesser solution to our quadratic, which represents the lower bandedge of our "peaking" response. We then have

$$\hat{\Omega} = \frac{\Omega_o}{\beta}(\Omega_c - \sqrt{\Omega_c^2 - \beta^2}) \tag{41}$$

By computing the pseudo-inverse of the matrix representation of this transform and applying it to a stabilized filter transformed by the peaking mapping in (36) we can generate a shelving filter.

The discrete-time peaking and shelving allpass transformation are shown in Figure 4. In both cases we choose $\omega_c = 0.3\pi$ and in the case of the peaking transformation $\hat{\omega}_o = \frac{\pi}{2}$.

5. DISCRETIZATION WITH CONFORMAL MAPS

We now apply the peaking and shelving conformal maps from the previous section to the task of adjusting and discretizing the response of filters with behavior near the Nyquist limit.

5.1. Discretization of an analog equalizer

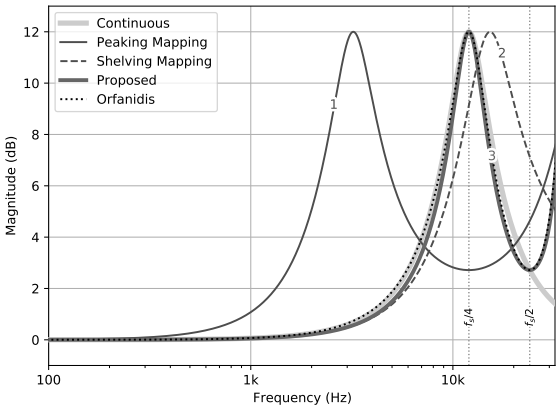

Figure 5: *Proposed discretization with steps corresponding to numbered curves in figure:*
1. We apply the peaking mapping with $\Omega_c = \Omega_s/2$ and $\Omega_o = \Omega_s/4$ to truncate the continuous response to $f_s/2$.
2. We then use the inverse mapping in (39) to generate a "shelving" filter whose peak is at the warped frequency in 42.
3. The "shelving" response is discretized using the bilinear transform and is a close match to the results in [18] and the original continuous response.

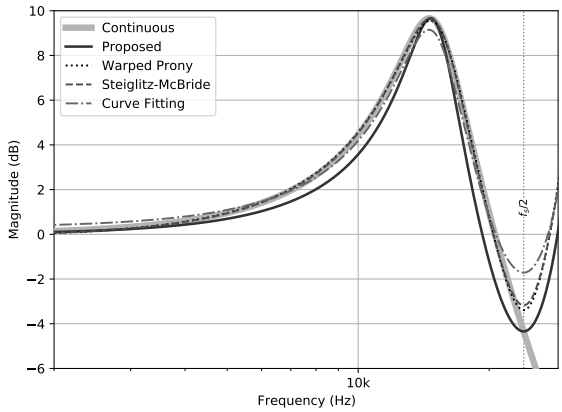

Figure 6: *Comparison of the proposed method to various optimization based filter design schemes.*

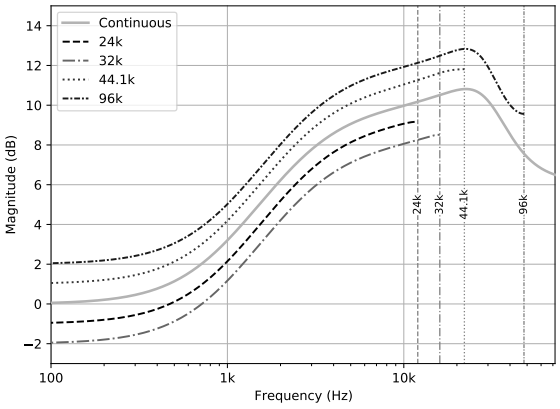

Figure 7: *Discretization of a single 4th-order analog response across multiple sampling rates, offset by ±1 and ±2 dB*

As an example, we examine the analog equalizer (5) from Sec. 2. To generate a similar result to [18], we need to truncate the original response to the Nyquist limit and then account for the effects of frequency warping. This is done by utilizing the continuous-time shelving conformal map to generate a truncated response that is also prewarped.

First, we apply the continuous-time lowpass-to-peaking transform by choosing $\Omega_c = \Omega_s/2$ and $\Omega_o = \Omega_s/4$, resulting in a 4th order filter mirrored about $f_s/4$ and where our original response is truncated at $f_s/2$. After stabilizing our filter, we then use the inverse of the mapping in (39) to generate our "shelving" response. As with [18], we choose $\beta = \Omega/4$ by evaluating the geometric mean of our poles.

To compensate for the bilinear transform warping, we choose $\hat{\beta}$ to be the prewarped digital frequency of β

$$\hat{\beta} = c \tan\left(\frac{\beta T}{2}\right) \tag{42}$$

Lastly, we discretize our shelving transformed filter with the bilinear transform to generate our matched digital response. This process is shown in Figure 5 as a series of three steps. The result of the proposed method is a digital filter whose response is a close match to the result in [18] and the original response.

As we double and then later halve the order of our system, the proposed method is order preserving. Unlike [18], the proposed method requires no knowledge of the original filter's construction and is parametrized by only f_s, Ω_o, Ω_c, and $\hat{\beta}$.

5.2. Comparison to optimization methods

In Figure 6, we utilize the proposed method to discetize the resonant lowpass filter originally shown in Figure 3 and compare the results to optimization schemes presented in [11–13]. The first two responses are formed using the Matlab library's `invfreqz` and `stmcb` methods.

While the proposed method's magnitude response deviates more from the continuous-time response compared to the warped Prony and Steiglitz-McBridge methods, the optimization methods shown require that a frequency and impulse response — truncated to $f_s/2$ — are precomputed to feed the optimization. In comparison, the proposed method only requires computation of the conformal mapping matrices and is parameterizable. A more exact match to the overall analog response could be derived by adjusting the proposed method's parameters in exchange for losing a perfect mapping at, say, the Nyquist limit.

5.3. Matched analog response across multiple sampling rates

The proposed method can be used to discretize the same analog filter across multiple sampling rates while maintaining the characteristic of the analog filter below each sampling rates' Nyquist limit. This is useful in the case we want to replicate the same response across different systems with different operating frequencies.

The filter we are discretizing is a 4th-order filter that is a cascade of a 2nd-order lowshelf section with of cutoff frequency of 10 kHz and 2nd-order highshelf section with a cutoff frequency of 30 kHz, both designed as defined in [4]. We choose 24kHz, 32kHz, 44.1kHz, and 96kHz as our operating frequencies to represent common audio sampling rates as well as lower sampling rates for embedded systems applications. As our Nyquist limit for the lower sampling rates truncate the full analog response, we similarly modify our choice of β to be below each Nyquist limit.

We choose to use the geometric mean of our poles to compute β, but limit our geometric mean to be the filter poles whose radii are below our Nyquist limit.

$$\beta = |(\prod_{i}^{N} p_i')^{1/N}| \tag{43}$$

where

$$p' = \{p_i : |p_i| < \pi f_s\} \tag{44}$$

The results of these discretizations are shown in Figure 7, demonstrating that the responses for all our desired operating frequencies are well matched to our continuous-time response below each operating frequency's Nyquist limit.

6. CONCLUSIONS AND FUTURE WORK

We have proposed a new parametrizable and order preserving discretization method based on conformal mapping and derived peaking and shelving conformal maps. Additionally, a method for inverting conformal maps based on their matrix operation on filter

coefficients has been demonstrated. The proposed method produces similar results when compared to other methods that directly modify the construction of a prototype filter and optimization methods based on a desired response. However, the proposed method is invariant to the original filter it is discretizing and can be parameterized based on the sampling rate and critical frequencies.

We believe the proposed method would be well applied to future work in analog modeling, where filters in units such as Wah-Wah pedals, EQs, and synthesizers have behavior near the Nyquist limit and are also time-varying. As the proposed method is parameterizable, discretization could be based on said time-varying parameters. The proposed method would also allow one model to run on many different systems using the technique from the previous section.

7. REFERENCES

[1] Stanley A. White, "Design of a digital biquadratic peaking or notch filter for digital audio equalization," in *Audio Engineering Society Convention 78*, May 1985.

[2] Juha Backman, "Digital realisation of phono (RIAA) equalisers," *IEEE Transactions on Consumer Electronics*, vol. 37, no. 3, pp. 659–662, 1991.

[3] François G. Germain and Kurt James Werner, "Optimizing differentiated discretization for audio circuits beyond driving point transfer functions," in *2017 IEEE Workshop on Applications of Signal Processing to Audio and Acoustics (WASPAA)*, 2017, pp. 384–388.

[4] Udo Zölzer, *Digital Audio Signal Processing*, John Wiley and Sons Ltd, Chippenham, England, 2 edition, 2008.

[5] Vesa Välimäki and Joshua D. Reiss, "All about audio equalization: Solutions and frontiers," *Applied Sciences*, vol. 6, no. 5, 2016.

[6] Julius O. Smith, *Introduction to Digital Filters with Audio Applications*, W3K Publishing, 2007.

[7] Tim Stilson, *Efficiently-Variable Non-Oversampled Algorithms in Virtual-Analog Music Synthesis*, Ph.D. thesis, Stanford University, 2006.

[8] Julius O. Smith and Jonathan S. Abel, "The bark bilinear transform," in *Proceedings of the IEEE Workshop on Applications of Signal Processing to Audio and Acoustics*, 1995, pp. 202–205.

[9] Julius O. Smith, *Physical Audio Signal Processing*, W3K Publishing, 2010.

[10] Atmadji Wiseso Soewito, *Least square digital filter design in the frequency domain*, Ph.D. thesis, Rice University, 1991.

[11] E.C. Levy, "Complex-curve fitting," *IRE Transactions on Automatic Control*, vol. AC-4, no. 1, pp. 37–43, 1959.

[12] Leland B. Jackson, "Frequency-domain Steiglitz-McBride method for least-squares IIR filter design, ARMA modeling, and periodogram smoothing," *IEEE Signal Processing Letters*, vol. 15, pp. 49–52, 2008.

[13] Matti Karjalainen, Aki Härmä, and Unto K. Laine, "Realizable warped IIR filters and their properties," in *1997 IEEE International Conference on Acoustics, Speech, and Signal Processing*, 1997, vol. 3, pp. 2205–2208.

[14] Simo Sarkka and Antti Huovilainen, "Accurate discretization of analog audio filters with application to parametric equalizer design," *IEEE Transactions on Audio, Speech, and Language Processing*, vol. 19, no. 8, pp. 2486–2493, 2011.

[15] David P. Berners and Jonathan S. Abel, "Discrete-time shelf filter design for analog modeling," in *Audio Engineering Society Convention 115*, Oct 2003.

[16] Juan Sierra, "Digital parametric filters beyond Nyquist frequency," in *Audio Engineering Society Convention 147*, http://www.aes.org/e-lib/browse.cfm?elib=20597, Oct 2019.

[17] Champ Darabundit and Russell Wedelich, "Generalized digital second order systems beyond Nyquist," in *Audio Engineering Society Convention 149*, Oct 2020.

[18] Sophocles J. Orfanidis, "Digital parametric equalizer design with prescribed Nyquist-frequency gain," *J. Audio Eng. Soc.*, vol. 34, pp. 444, June 1997.

[19] Michael Massberg, "Digital low-pass filter design with analog-matched magnitude response," in *Audio Engineering Society Convention 131*, October 2011.

[20] Zeev Nehari, *Conformal Mapping*, Dover Publications Inc., 1952.

[21] François G. Germain and Kurt J Werner, "Design principles for lumped model discretisation using Möbius transforms," in *Proc. Digital Audio Effects (DAFx-15)*, Trondheim, Norway, Nov. 30 - Dec. 3 2015.

[22] Matti Karjalainen, Aki Härmä, Unto K. Laine, and Jyri Huopaniemi, "Warped filters and their audio applications," in *Proceedings of 1997 Workshop on Applications of Signal Processing to Audio and Acoustics*, 1997.

[23] Elmar Krüger and Hans Werner Strube, "Linear prediction on a warped frequency scale (speech processing)," *IEEE Transactions on Acoustics, Speech, and Signal Processing*, vol. 36, no. 9, pp. 1529–1531, 1988.

[24] A. G. Constantinides, "Spectral transformations for digital filters," in *Proc. The Institution of Electrical Engineers*, August 1970, vol. 117, pp. 1585–1590.

[25] Ernst A Guillemin, *Synthesis of passive networks; theory and methods appropriate to the realization and approximation problems*, John Wiley and Sons Ltd, 1957.

[26] James A. Moorer, "The manifold joys of conformal mapping: Applications to digital filtering in the studio," *J. Audio Eng. Soc.*, vol. 31, no. 11, pp. 826–841, November 1983.

[27] Aubrey M. Bush and Daniel C. Fielder, "Simplified algebra for the bilinear and related transformations," *IEEE Transactions on Audio and Electroacoustics*, vol. 21, no. 2, pp. 127–128, 1973.

[28] Markus Lang and Timo I. Laakso, "Simple and robust method for the design of allpass filters using least-squares phase error criterion," *IEEE Transactions on Circuits and Systems II: Analog and Digital Signal Processing*, vol. 41, no. 1, pp. 40–48, 1994.

[29] Sophocles J. Orfanidis, "High-order digital parametric equalizer design," in *J. Audio Eng. Soc.*, November 2005, vol. 53, pp. 1026–1024.